Perovskites Hot Paper

Deutsche Ausgabe: DOI: 10.1002/ange.201411956
Internationale Ausgabe: DOI: 10.1002/anie.201411956

Self-Template-Directed Synthesis of Porous Perovskite Nanowires at Room Temperature for High-Performance Visible-Light Photodetectors**

*Sifei Zhuo, Jingfang Zhang, Yanmei Shi, Yi Huang, and Bin Zhang**

Abstract: *The unique optoelectronic properties and promising photovoltaic applications of organolead halide perovskites have driven the exploration of facile strategies to synthesize organometal halide perovskites and corresponding hybrid materials and devices. Currently, the preparation of $CH_3NH_3PbBr_3$ perovskite nanowires, especially those with porous features, is still a great challenge. An efficient self-template-directed synthesis of high-quality porous $CH_3NH_3PbBr_3$ perovskite nanowires in solution at room temperature using the Pb-containing precursor nanowires as both the sacrificial template and the Pb^{2+} source in the presence of CH_3NH_3Br and HBr is now presented. The initial formation of $CH_3NH_3PbBr_3$ perovskite layers on the surface of the precursor nanowires and the following dissolution of the organic component of the latter led to the formation of mesopores and the preservation of the 1D morphology. Furthermore, the perovskite nanowires are potential materials for visible-light photodetectors with high sensitivity and stability.*

Organolead halide perovskites with a typical formula of $(CH_3NH_3)PbX_3$ (X = I, Br, or Cl) have experienced rapid development in the field of solar cells since 2009.[1–3] In the beginning, organolead halide perovskite were used as light absorbers that were deposited on mesoporous scaffolds in sensitized solar cells.[1a,2] Subsequently, researchers demonstrated that organolead halide perovskites also transport both positive and negative photoinduced charge carriers with long diffusion lengths and lifetimes in planar heterojunction perovskite solar cells, which opened new opportunities for organolead halide perovskites in film solar cells as well as potential applications in optical, electronic, and optoelectronic fields.[3] The superior optical absorption combined with the long-range electron–hole diffusion length of the organolead halide perovskites are driving the exploration of synthetic approaches to control their morphology and structure and explore new applications.[4] For instance, various inks of 6 nm-sized $CH_3NH_3PbBr_3$ perovskite nanoparticles have been reported by Pérez-Prieto and co-workers.[4a] Nanoporous $CH_3NH_3PbI_3$ single crystals were prepared by a well-designed crystal-to-crystal transformation.[4b] Compared to their bulk counterparts, nanoscale organolead halide perovskites may show an improved performance in nanoscale solar cells and other nanodevices because of the small-size effect, especially with the peculiar geometrical configuration.

Porous nanomaterials have attracted increasing attention owing to their improved physical and chemical properties compared with their corresponding solid counterparts.[5] Meanwhile, nanowires were shown to have excellent performance and applications in electronics, photoelectronics, and sensors because of the anisotropic geometry or enhanced light absorption, which may be modulated by synthetic control of the morphology and chemical composition.[6] The unique porous structure and 1D configuration of nanoporous nanowires can shorten the transport distance of ions, electrons, and holes, have many active sites on their surface, and hence exhibit high activity in catalysts,[7] energy storage,[8] and gas sensors.[9] Thus, nanoporous perovskite nanowires may be used in advanced electronic and photoelectronic applications because they can combine a variety of advantages of organolead halide perovskites and 1D porous materials. However, the very rapid reaction between Pb^{2+} ions and HBr/CH_3NH_3Br makes the controlled synthesis of organolead halide perovskite nanomaterials, especially of porous and 1D structures, highly challenging.

Herein, we report the facile self-template-directed fabrication of porous $CH_3NH_3PbBr_3$ perovskite nanowires through the reaction of Pb-containing precursor nanowires with CH_3NH_3Br and HBr in an organic solvent at room temperature. In this chemical transformation, Pb-containing precursor nanowires were quickly converted into $CH_3NH_3PbBr_3$ with preserved macroscopic 1D morphology by the initial formation of the perovskite as a protective layer on the surface of the precursor nanowires. The release of the organic component of the precursor nanowires into the solvent led to the formation of mesopores in the $CH_3NH_3PbBr_3$ nanowires. In addition, we show that the porous $CH_3NH_3PbBr_3$ nanowires can be used as visible-light photodetectors with high stability and sensitivity. The porous 1D organolead halide perovskites may be applied in the field of single-nanowire solar cells and photoelectric devices.

The Pb-containing precursor nanowires were fabricated by a method based on cysteine coordination reported by Zhang and coworkers.[10] The morphology and structure of the nanowires were first determined by scanning electron microscopy (SEM) and transmission electron microscopy (TEM). Typical SEM images (Figure 1a,b) show that the

[*] S. Zhuo, J. Zhang, Y. Shi, Y. Huang, Prof. Dr. B. Zhang
Department of Chemistry, School of Science, Tianjin University, and Collaborative Innovation Center of Chemical Science and Engineering (Tianjin)
Tianjin 300072 (P.R. China)
E-mail: bzhang@tju.edu.cn

[**] This work was financially supported by the National Natural Science Foundation of China (No. 21422104).

Supporting information for this article is available on the WWW under http://dx.doi.org/10.1002/anie.201411956.

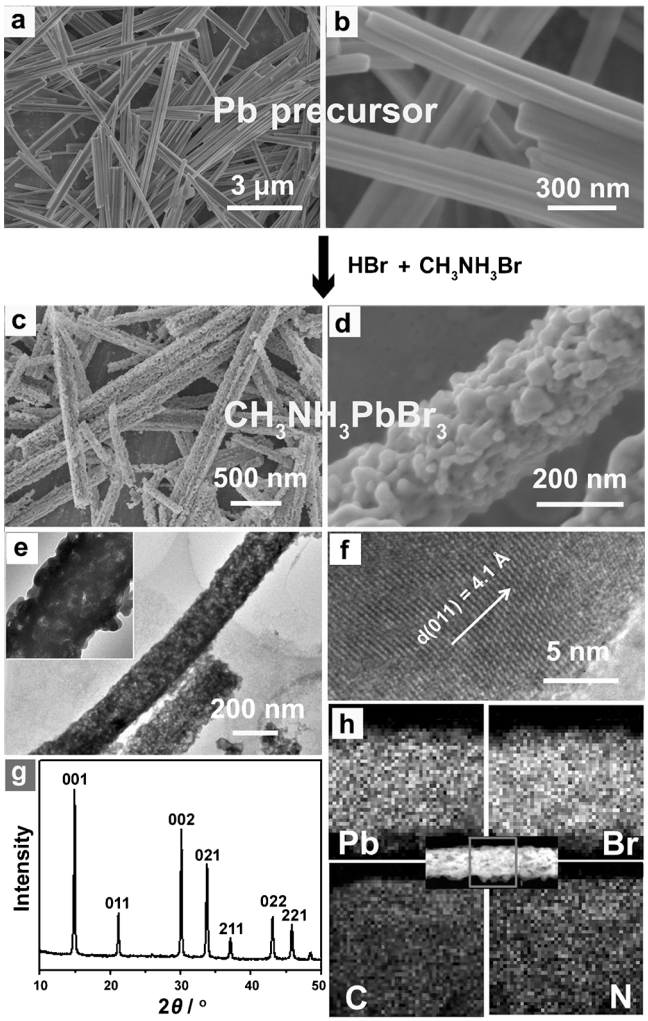

Figure 1. a, b) SEM images of the Pb-containing precursor nanowires. c, d) SEM images, e) TEM images, f) HRTEM image, g) XRD pattern, and h) STEM-EDS elemental mapping of the porous $CH_3NH_3PbBr_3$ perovskite nanowires.

Pb-containing nanowires were successfully synthesized with a length of about 10 μm and a diameter of around 200 nm. The TEM and associated high-resolution TEM (HRTEM) images (Figure S1 a,b in the Supporting Information) indicate that the solid nanowires are comprised of nanocrystals that are smaller than 5 nm in diameter. Furthermore, the X-ray diffraction (XRD) pattern (Figure S1c) and the point-scan energy-dispersive X-ray spectroscopic analysis (EDS) spectrum (Figure S1d) show that the precursor nanowires are well crystallized and composed of Pb, C, N, O, and S. Although the determination of the exact crystal structure of the nanowires was difficult, we concluded that these Pb^{2+}-coordinating hybrid nanowires can be fabricated.

The Pb-containing precursor nanowires were used as both template and Pb^{2+} ion source for the reaction with CH_3NH_3Br and HBr in 2-propanol at room temperature. (see the Supporting Information for details). Typical SEM images (Figure 1 c,d) show that the corresponding products are nanowires with a relatively rough surface, suggesting that the 1D morphology of the Pb-containing precursors can be retained after such a self-template-directed chemical transformation. The TEM image in Figure 1 e indicates that the obtained samples are porous nanowires comprised of nanoparticles. Furthermore, all the diffraction peaks in the XRD pattern (Figure 1 g) can be assigned to a cubic $CH_3NH_3PbBr_3$ structure[1a,4a] with high purity and good crystallinity, and the HRTEM image (Figure 1 f) shows a well-defined lattice spacing consistent with the XRD pattern. Additionally, scanning transmission electron microscopy energy dispersive spectroscopy (STEM-EDS) elemental mapping images (Figure 1 h) indicate the uniform distribution of Pb, Br, C, and N in the porous $CH_3NH_3PbBr_3$ perovskite nanowires. These results clearly demonstrate that the solid precursor nanowires have been successfully transformed into porous nanowires with retention of their macroscopic 1D morphology (Figure S2).

To understand the mechanism of the chemical transformation of solid Pb^{2+}-coordinating precursor nanowires to porous $CH_3NH_3PbBr_3$ nanowires, SEM, TEM, EDS, and XRD analyses were adopted. The morphological evolution and crystal transition process were illustrated by examining the intermediates collected at different stages of the chemical transformation. After the rapid addition of a dispersion of the precursor nanowires to a solution with an excess of HBr and CH_3NH_3Br, the color of the dispersion changed from white to yellow within a second. XRD pattern (Figure 2 i) and EDS spectra (Figure S5b) show that the precursor nanowires were partially converted to $CH_3NH_3PbBr_3$ perovskites. SEM (Figure 2 c) and TEM images (Figure 2 f and Figure S3a) show that the precursor nanowires were quickly covered with layers of $CH_3NH_3PbBr_3$ perovskites, whereas the interior remained solid Pb-containing nanowires. The release and dissolution of organic components of the precursors lead to the formation of pores in the shell, as shown in Figure 2 f and Figures S3 and S4, thus helping the following internal conversion of the precursor nanowires. The Br distribution by EDS line analysis (Figure S3c) confirmed the core–shell structure of the intermediates. With an increasing reaction time, the signals of the precursors became weaker, and those of the perovskite became stronger (Figure 2 i,j and Figure S5), while the pores became more and more obvious on the surface of the layer (Figure S4 and Figure 2 d,g). The result confirms the gradual outside-to-inside transformation of the solid Pb-containing nanowires to porous $CH_3NH_3PbBr_3$ nanowires. A prolonged reaction time eventually led to the generation of porous $CH_3NH_3PbBr_3$ perovskite nanowires with high purity and crystallinity. By contrast, when we added HBr slowly to the mixture of precursors and CH_3NH_3Br, irregular nanosized bulks were formed on the surface of the precursors without protective layers and finally led to the formation of $CH_3NH_3PbBr_3$ macrosized bulks rather than porous nanowires (Figure S6). Furthermore, in the absence of CH_3NH_3Br, but otherwise unchanged conditions, the samples are $PbBr_2$ bulks instead of nanowires (Figure S7). These results suggest that the mechanism for the transformation of solid Pb-containing nanowires to porous $CH_3NH_3PbBr_3$ perovskite nanowires involves a self-template-directed reaction with HBr and CH_3NH_3Br accompanied by the dissolution of organic components into the solvent (Figure 2 a). First,

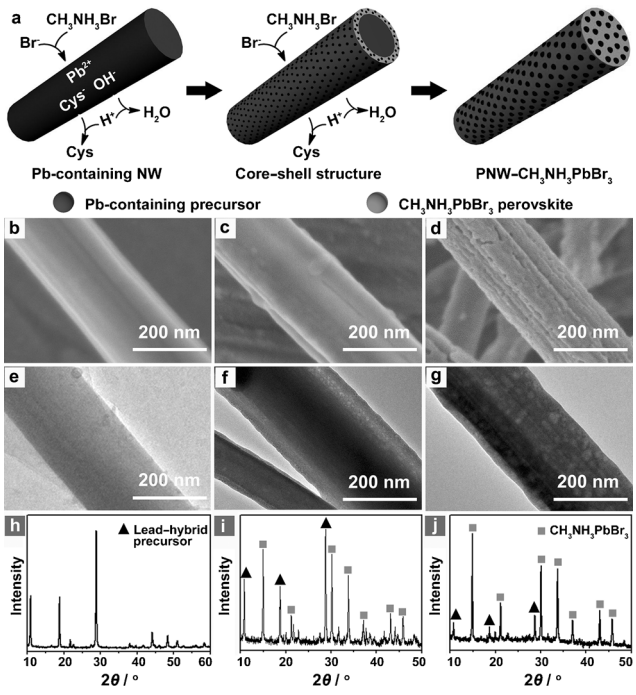

Figure 2. a) Synthesis of porous $CH_3NH_3PbBr_3$ nanowires (PNW-$CH_3NH_3PbBr_3$) through the self-template-directed chemical transformation of the Pb-containing precursor nanowires. b–d) SEM images, e–g) TEM images, and h–j) XRD patterns of the intermediates at different reaction times: 0 min (b, e, h), 1 min (c, f, i), 60 min (d, g, j).

$CH_3NH_3PbBr_3$ perovskite layers were formed on the surface of the Pb-containing nanowires owing to the high chemical reactivity of Pb^{2+} with HBr and CH_3NH_3Br to produce $CH_3NH_3PbBr_3$. The unique perovskite layers play a key role in the preservation of the 1D nanostructure by protecting the precursor nanowires from attack by HBr and CH_3NH_3Br. Then, the nanopores in the shell, which originated from the dissolution of the organic component of the precursors into the solvent,[7a] may enable the inward diffusion of HBr and CH_3NH_3Br and the subsequent reaction with Pb^{2+} species in the interior of the wire-like precursors. Accompanied by this reaction process, the continuous dissolution and diffusion of the organic component of the hybrid nanowires led to the production of mesopores in the final 1D $CH_3NH_3PbBr_3$ perovskite products. In addition, the products were nanoparticles rather than porous nanowires when the 2-propanol was replaced by ethyl acetate. This phenomenon may be due to the poor solubility of CH_3NH_3Br in ethyl acetate (Figure S8), which may offer an effective and alternative way to prepare $CH_3NH_3PbBr_3$ nanoparticles by choosing the suitable reaction medium. We expect that this self-template-directed synthesis may be extended to the fabrication of other nanoporous perovskite 1D nanowires and nanoparticles.

Recently, great efforts have been devoted to the exploitation of nanowire devices (e.g. Si, GaN, CdS) for a variety of applications.[11] Now, organolead halide perovskites have been identified as promising materials for future solar cells, light-emitting diodes, lasers, ferroelectrics, and fluorescence probes.[12] Thus, we investigated the optoelectronic properties of the porous $CH_3NH_3PbBr_3$ nanowires as visible-light

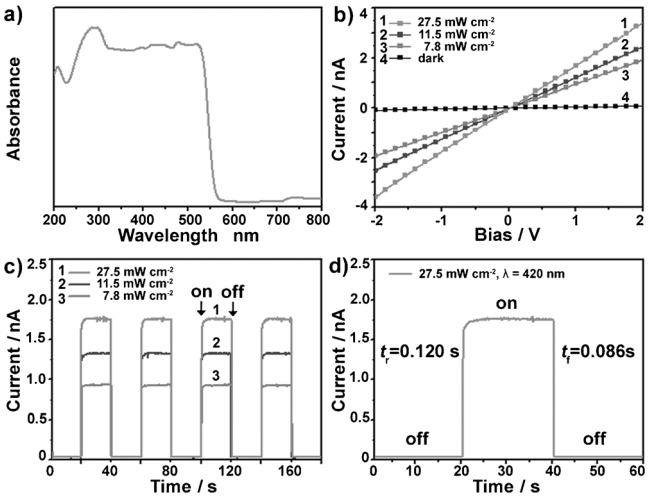

Figure 3. a) UV/Vis absorption spectrum, b) typical *I–V* curves, and c, d) photoreponse at 1 V of the porous $CH_3NH_3PbBr_3$ nanowires under 420 nm light irradiation.

photodetectors. The UV/Vis absorption spectrum (Figure 3a) indicates that the porous $CH_3NH_3PbBr_3$ nanowires have a favorable absorption capability with a direct band gap about 2.22 eV, measured from the transformed Kubelka–Munk spectrum (Figure S9), coinciding well with the previous report.[2d] Then, the optoelectronic properties were studied on a gold interdigital electrode with adjacent intervals of about 150 μm. Upon illumination with a 420 nm laser, the typical linear and symmetrical photocurrent versus voltage (*I–V*) plots (Figure 3b) indicate that the porous $CH_3NH_3PbBr_3$ nanowires are dispersed on the interdigital electrode with good ohmic contact.[13] Figure 3b shows the increase of the optoelectronic current of porous $CH_3NH_3PbBr_3$ nanowires with a higher light intensity. Irradiation with light of a wavelength of 420 nm and at different intensities (7.8, 11.5, and 27.5 $mW\,cm^{-2}$) at an applied voltage of 1 V led to a superior photocurrent response of the porous $CH_3NH_3PbBr_3$ nanowire electrode with the current ON/OFF ratios of 30.6, 46.8, and 61.9, respectively (Figure 3c), thus illustrating a good response to the light intensity. Furthermore, the photoresponse time (Figure 3d), which is one of the key criteria for detection performance, is as fast as 0.12 s, and the decay time is estimated to be about 0.086 s, both of which are superior to those of multiple other semiconductors (Table S1). In addition, the high stability and reproducibility of the photoelectronic response at various bias potentials further imply that the porous $CH_3NH_3PbBr_3$ nanowires are promising materials for optoelectronic devices (Figure S10 and 11). The promising optoelectronic performance of the porous $CH_3NH_3PbBr_3$ nanowires may be associated with the 1D porous configuration, enhanced light absorption, and the unique nature of the organolead halide perovskites. It is reasonable to anticipate that the 1D porous geometry and optoelectronic performance of organolead halide perovskite nanowires will extend the scope of applications in nanoscale solar cells and nanodevices after being further functionalized to form heterostructures.[14]

In summary, we have demonstrated a facile method for the preparation of porous $CH_3NH_3PbBr_3$ perovskite nanowires by a self-template-directed reaction of Pb-containing nanowires with HBr and CH_3NH_3Br at room temperature in solution. The initial formation of $CH_3NH_3PbBr_3$ perovskite layers on the surface of the precursor nanowires and the following dissolution of the organic component of the Pb-containing precursor nanowires are considered to play an important role in the production of the porous wire-like perovskite nanostructures with preserving the 1D macrostructure. By changing the solvent, this method is also suitable for the generation of $CH_3NH_3PbBr_3$ perovskite nanoparticles. Furthermore, the porous $CH_3NH_3PbBr_3$ nanowires exhibit superior optoelectronic activity as visible-light photodetectors with a photoresponse time of only 0.12 s and a decay time of about 0.086 s. The high sensitivity and stability of porous organolead perovskite nanowires may be attributed to the unique porous 1D geometry, many active sites, and good ability to absorb light. In addition, considering the unique porous 1D geometry and the superior optoelectronic performance of organolead halide perovskite, our facile self-template-directed synthetic approach may result in nanoporous $CH_3NH_3PbBr_3$ nanowire as promising substrates for the fabrication of high-performance single nanowire solar cells and photoelectric devices by creating heteroepitaxial junctions or coaxial structures (Figure S12).[15]

Keywords: nanowires · perovskites · photodectors · porous materials · self-template

How to cite: *Angew. Chem. Int. Ed.* **2015**, *54*, 5693–5696
Angew. Chem. **2015**, *127*, 5785–5788

[1] a) A. Kojima, K. Teshima, Y. Shirai, T. Miyasaka, *J. Am. Chem. Soc.* **2009**, *131*, 6050; b) M. D. McGehee, *Nature* **2013**, *501*, 323; c) G. Hodes, *Science* **2013**, *342*, 317; d) P. Gao, M. Grätzel, M. K. Nazeeruddin, *Energy Environ. Sci.* **2014**, *7*, 2448.

[2] a) J. H. Im, C. R. Lee, J. W. Lee, S. W. Park, N. G. Park, *Nanoscale* **2011**, *3*, 4088; b) M. M. Lee, J. Teuscher, T. Miyasaka, T. N. Murakami, H. J. Snaith, *Science* **2012**, *338*, 643; c) J. Burschka, N. Pellet, S. J. Moon, R. Humphry-Baker, P. Gao, M. K. Nazeeruddin, M. Grätzel, *Nature* **2013**, *499*, 316; d) J. H. Noh, S. H. Im, J. H. Heo, T. N. Mandal, S. I. Seok, *Nano Lett.* **2013**, *13*, 1764.

[3] a) M. Liu, M. B. Johnston, H. J. Snaith, *Nature* **2013**, *501*, 395; b) S. D. Stranks, G. E. Eperon, G. Grancini, C. Menelaou, M. J. P. Alcocer, T. Leijtens, L. M. Herz, A. Petrozza, H. J. Snaith, *Science* **2013**, *342*, 341; c) G. Xing, N. Mathews, S. Sun, S. S. Lim, Y. M. Lam, M. Grätzel, S. Mhaisalkar, T. C. Sum, *Science* **2013**, *342*, 344; d) H. Zhou, Q. Chen, G. Li, S. Luo, T. B. Song, H. S. Duan, Z. Hong, J. You, Y. Liu, Y. Yang, *Science* **2014**, *345*, 542.

[4] a) L. C. Schmidt, A. Pertegás, S. González-Carrero, O. Malinkiewicz, S. Agouram, G. Mínguez Espallargas, H. J. Bolink, R. E. Galian, J. Pérez-Prieto, *J. Am. Chem. Soc.* **2014**, *136*, 850; b) T. Kollek, D. Gruber, J. Gehring, E. Zimmermann, L. Schmidt-Mende, S. Polarz, *Angew. Chem. Int. Ed.* **2015**, *54*, 1341; *Angew. Chem.* **2015**, *127*, 1357.

[5] a) L. Zhang, H. B. Wu, Y. Yan, X. Wang, X. W. Lou, *Energy Environ. Sci.* **2014**, *7*, 3302; b) E. V. Skorb, D. V. Andreeva, H. Möhwald, *Angew. Chem. Int. Ed.* **2012**, *51*, 5138; *Angew. Chem.* **2012**, *124*, 5228; c) J. B. Joo, M. Dahl, N. Li, F. Zaera, Y. Yin, *Energy Environ. Sci.* **2013**, *6*, 2082; d) W. Zhang, Z. Y. Wu, H. L. Jiang, S. H. Yu, *J. Am. Chem. Soc.* **2014**, *136*, 14385.

[6] a) S. K. Kim, K. D. Song, T. J. Kempa, R. W. Day, C. M. Lieber, H. G. Park, *ACS Nano* **2014**, *8*, 3707; b) R. Yan, D. Gargas, P. Yang, *Nat. Photonics* **2009**, *3*, 569.

[7] a) S. Zhuo, Y. Xu, W. Zhao, J. Zhang, B. Zhang, *Angew. Chem. Int. Ed.* **2013**, *52*, 8602; *Angew. Chem.* **2013**, *125*, 8764; b) T. Y. Ma, S. Dai, M. Jaroniec, S. Z. Qiao, *J. Am. Chem. Soc.* **2014**, *136*, 13925.

[8] a) X. Zhang, F. Cheng, J. Yang, J. Chen, *Nano Lett.* **2013**, *13*, 2822; b) J. P. Alper, S. Wang, F. Rossi, G. Salviati, N. Yiu, C. Carraro, R. Maboudian, *Nano Lett.* **2014**, *14*, 1843.

[9] D. Yang, L. F. Fonseca, *Nano Lett.* **2013**, *13*, 5642.

[10] H. Tong, Y. J. Zhu, L. X. Yang, L. Li, L. Zhang, *Angew. Chem. Int. Ed.* **2006**, *45*, 7739; *Angew. Chem.* **2006**, *118*, 7903.

[11] a) Z. L. Wang, J. Song, *Science* **2006**, *312*, 242; b) T. J. Kempa, R. W. Day, S. K. Kim, H. G. Park, C. M. Lieber, *Energy Environ. Sci.* **2013**, *6*, 719.

[12] a) Z. K. Tan, R. S. Moghaddam, M. L. Lai, P. Docampo, R. Higler, F. Deschler, M. Price, A. Sadhanala, L. M. Pazos, D. Credgington, F. Hanusch, T. Bein, H. J. Snaith, R. H. Friend, *Nat. Nanotechnol.* **2014**, *9*, 687; b) G. Xing, N. Mathews, S. S. Lim, N. Yantara, X. Liu, D. Sabba, M. Grätzel, S. Mhaisalkar, T. C. Sum, *Nat. Mater.* **2014**, *13*, 476; c) Y. Kutes, L. Ye, Y. Zhou, S. Pang, B. D. Huey, N. P. Padture, *J. Phys. Chem. Lett.* **2014**, *5*, 3335; d) Y. Niu, F. Zhang, Z. Bai, Y. Dong, J. Yang, R. Liu, B. Zou, J. Li, H. Zhong, *Adv. Opt. Mater.* **2015**, *3*, 112.

[13] a) G. Chen, Z. Liu, B. Liang, G. Yu, Z. Xie, H. Huang, B. Liu, X. Wang, D. Chen, M. Q. Zhu, G. Shen, *Adv. Funct. Mater.* **2013**, *23*, 2681; b) X. Hu, X. Zhang, L. Liang, J. Bao, S. Li, W. Yang, Y. Xie, *Adv. Funct. Mater.* **2014**, *24*, 7373.

[14] a) J. J. Wang, T. Ling, S. Z. Qiao, X. W. Du, *ACS Appl. Mater. Interfaces* **2014**, *6*, 14718; b) K. Deng, L. Li, *Adv. Mater.* **2014**, *26*, 2619.

[15] a) B. Tian, X. Zheng, T. J. Kempa, Y. Fang, N. Yu, G. Yu, J. Huang, C. M. Lieber, *Nature* **2007**, *449*, 885; b) Z. Li, Z. Hu, J. Peng, C. Wu, Y. Yang, F. Feng, P. Gao, J. Yang, Y. Xie, *Adv. Funct. Mater.* **2014**, *24*, 1821; c) C. Xie, B. Nie, L. Zeng, F. X. Liang, M. Z. Wang, L. Luo, M. Feng, Y. Yu, C. Y. Wu, Y. Wu, S. H. Yu, *ACS Nano* **2014**, *8*, 4015.

Received: December 12, 2014
Published online: March 16, 2015

